PNAS RESEARCH ARTICLE | PHYSICS

A model of *d*-wave superconductivity, antiferromagnetism, and charge order on the square lattice

Maine Christos[a], Zhu-Xi Luo[a], Henry Shackleton[a,b], Ya-Hui Zhang[c], Mathias S. Scheurer[d], and Subir Sachdev[a,1]

Contributed by Subir Sachdev; received February 16, 2023; accepted April 15, 2023; reviewed by Yin-Chen He and Yasir Iqbal

We describe the confining instabilities of a proposed quantum spin liquid underlying the pseudogap metal state of the hole-doped cuprates. The spin liquid can be described by a SU(2) gauge theory of $N_f = 2$ massless Dirac fermions carrying fundamental gauge charges—this is the low-energy theory of a mean-field state of fermionic spinons moving on the square lattice with π-flux per plaquette in the $\mathbb{Z}_2$ center of SU(2). This theory has an emergent $SO(5)_f$ global symmetry and is presumed to confine at low energies to the Néel state. At nonzero doping (or smaller Hubbard repulsion U at half-filling), we argue that confinement occurs via the Higgs condensation of bosonic chargons carrying fundamental SU(2) gauge charges also moving in π $\mathbb{Z}_2$-flux. At half-filling, the low-energy theory of the Higgs sector has $N_b = 2$ relativistic bosons with a possible emergent $SO(5)_b$ global symmetry describing rotations between a *d*-wave superconductor, period-2 charge stripes, and the time-reversal breaking "*d*-density wave" state. We propose a conformal SU(2) gauge theory with $N_f = 2$ fundamental fermions, $N_b = 2$ fundamental bosons, and a $SO(5)_f \times SO(5)_b$ global symmetry, which describes a deconfined quantum critical point between a confining state which breaks $SO(5)_f$ and a confining state which breaks $SO(5)_b$. The pattern of symmetry breaking within both SO(5)s is determined by terms likely irrelevant at the critical point, which can be chosen to obtain a transition between Néel order and *d*-wave superconductivity. A similar theory applies at nonzero doping and large U, with longer-range couplings of the chargons leading to charge order with longer periods.

spin liquid | superconductivity | charge order | quantum criticality

The phase diagram of the hole-doped cuprate compounds has been extensively studied in numerous careful experiments in recent decades, and a remarkably rich picture has emerged of the quantum phases of matter around the dome of high-temperature superconductivity (1). We present a theoretical approach to these phases designed to address the following key puzzles:

1. The pseudogap metal (found at intermediate temperatures and low doping) has a suppressed spin spectral weight and a photoemission gap in the antinodal region of the Brillouin zone. There is a puzzling "Fermi-arc" spectrum in the nodal region of the Brillouin zone (2, 3), not interpretable in terms of band theory.
2. The quantum oscillations observed at low temperatures and high magnetic fields in $YBa_2Cu_3O_{6.5}$ (4) appear to have an interpretation in terms of electron pockets induced by charge density wave order (5). However, computations of the reconstruction of the Fermi surface of the Fermi liquid state by charge order also predict additional gapless electronic excitations in the antinodal region of the Brillouin zone (6) which have not been observed.
3. The temperature scales of the *d*-wave superconductivity and the charge density wave orders are very similar to each other (7), suggesting a common origin. In Fermi liquid theory, the instabilities to such orders are determined by different interactions, and there is no particular reason for them to be similar.

Our theory begins (Fig. 1) with the assumption that the Fermi-arc spectrum in the pseudogap arises from an underlying pocket Fermi surface of electron-like particles of charge e and spin-1/2 (12–25) but with anisotropic spectral weight. This pocket Fermi surface encloses a volume which does not equal the free electron Luttinger value, and such a violation requires the presence of a spin liquid with fractionalized excitations, a state called the fractionalized Fermi liquid (FL*) in refs. 26 and 27. We will further assume that the spin liquid underlying the pseudogap metal is the popular π-flux state of fermionic spinons (28). As we will discuss below, although this π-flux state is now known to be ultimately unstable at $T = 0$, there is significant evidence for its stability

Significance

The cuprate compounds exhibit high-temperature superconductivity at ambient pressure and a complex phase diagram. Early studies proposed a connection between cuprate superconductivity and spin-liquid states characterized by excitations with fractionalized quantum numbers. But no direct evidence for fractionalization has since emerged, and the low-temperature phase diagram is dominated by a competition between superconductivity and charge-ordered states which break translational symmetry. Our theory uncovers features associated with a particular spin liquid presumed to underlie the higher temperature pseudogap metal phase and shows that it has multiple nearly degenerate instabilities to confinement of fractionalized excitations, leading to antiferromagnetism, *d*-wave superconductivity, and/or charge order. Our theory provides routes to resolving a number of open puzzles on the cuprate phase diagram.

Author contributions: M.C., Z.-X.L., H.S., Y.-H.Z., M.S.S., and S.S. designed research; M.C., Z.-X.L., H.S., Y.-H.Z., M.S.S., and S.S. performed research; and M.C., Z.-X.L., H.S., M.S.S., and S.S. wrote the paper.

Reviewers: Y.-C.H., Perimeter Institute; and Y.I., Indian Institute of Technology Madras.

The authors declare no competing interest.

[1]To whom correspondence may be addressed. Email: sachdev@g.harvard.edu.

This article contains supporting information online at https://www.pnas.org/lookup/suppl/doi:10.1073/pnas.2302701120/-/DCSupplemental.

Published May 16, 2023.

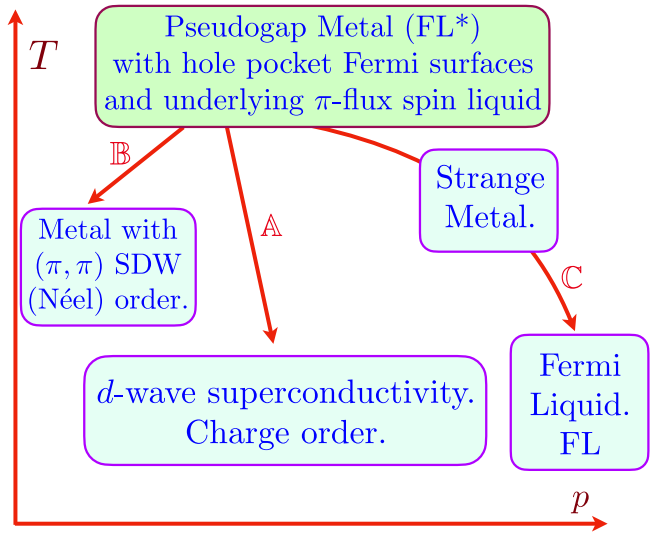

Fig. 1. Schematic phase diagram of the hole-doped cuprates as a function of temperature (T) and doping (p), with the pseudogap metal as the parent state for the cuprate phase diagram. The main analysis of the present paper concerns the transition to confining states from the π-flux spin liquid along arrow $\mathbb{A}$. The physics along arrow $\mathbb{B}$ is described using the bosonic spinon CP^1 theory in ref. 8. But arrow $\mathbb{B}$ is also described in the present paper in a dual theory by the confinement of fermionic spinons and gapped bosonic chargons as in Fig. 2. The physics along arrow $\mathbb{C}$ is discussed in refs. 9, 10, and 11.

over intermediate length scales, and so, it can describe fractionalized excitations at the pseudogap temperatures. Wang et al. (29) have argued that this π-flux state is dual to the critical point of another popular spin-liquid state, that is described by the CP^1 model of bosonic spinons (30). The bosonic spinon model is a useful starting point toward studying a confining instability to Néel order (8). Here, we shall exploit the fermionic spinon description to study confinement to charge order and superconductivity, as schematically sketched by arrow $\mathbb{A}$ in Fig. 1.

The π-flux spin liquid is a theory of fermionic spinons coupled as fundamentals to an emergent SU(2) gauge field (31, 32) and moving in a background of gauge-invariant π-flux in the $\mathbb{Z}_2$ center of SU(2). At low energies, the fermionic spectrum reduces to that of $N_f = 2$ massless Dirac fermions whose quadratic action has an emergent $SO(5)_f$ global symmetry (29, 33–37) (here the subscript f is only an identifying label specifying that the SO(5) acts on fermionic spinons). To obtain the superconducting and charge-ordered states, we will condense a Higgs field B a "chargon" (13–15), which is a fundamental of SU(2) and also carries a unit U(1) charge of electromagnetism (this U(1) is treated as effectively global). The boson B is a spin singlet under the SU(2) global spin rotation, while the fermionic spinons carry spin 1/2.

Several earlier works have considered the close relationship between the π-flux spin liquid and the d-wave superconductor (13–15, 31, 38–43). However, they assumed that the analog of the boson B carried all of the doping density and condensed in a spatially uniform manner in the d-wave superconductor. In our approach, the doping density is carried entirely by the electron-like hole pockets responsible for the observed Fermi arcs. This is especially clear in the ancilla formulation of the pseudogap metal phase (8–10, 24, 44), which we discuss in *SI Appendix*, section 1 (but in principle, as our presentation will show, all the results of the present paper can be obtained without the ancilla method). Consequently, B should be treated as a nearly relativistic Higgs boson or a "slave rotor" (45), rather than a nearly free nonrelativistic boson which undergoes Bose–Einstein condensation. Indeed, the ancilla approach involves a change in perspective on the physical interpretation of B: In earlier approaches (15), B was obtained by fractionalizing the electron into a spinon and a chargon B. In our approach, B is regarded as a composite of the spinon and the physical electron, as in Eq. **6**. But, at the level of symmetry and emergent gauge fields, there is no fundamental difference between the two approaches.

Furthermore, while the earlier works recognized that B carries a fundamental SU(2) gauge charge, this is a property of the gauge structure crucial to our analysis that has not been accentuated earlier. Like the fermionic spinons, the B bosons also move in a background of π-flux in the $\mathbb{Z}_2$ center of SU(2). This follows immediately from the facts that B is a composite of the physical electron and a spinon, and the electron cannot experience any emergent flux. This π-flux is SU(2) gauge-invariant, and choosing a gauge in which the π-flux spin liquid is transformed (31, 41, 42) into one with d-wave pairing between the spinons does not remove the $\mathbb{Z}_2$ flux. A key consequence of the $\mathbb{Z}_2$ flux is that the dispersion of the B must have at least two degenerate minima (46). (The works refs. 13, 14, and 15 employed a distinct "staggered flux" U(1) spin liquid for the pseudogap at nonzero doping, for which this additional degeneracy does not apply—*SI Appendix*, 5.) For the simplest case with only two minima, the low-energy theory in the vicinities of these minima yields a continuum theory with $N_b = 2$ flavors of bosons carrying fundamental SU(2) gauge charges. For reasons similar to the fermionic sector, the static action of this low-energy bosonic theory can have an emergent $SO(5)_b$ symmetry (where b is an identifying label to distinguish from the distinct $SO(5)_f$ symmetry). Degenerate bosonic minima and a $SO(5)_b$ symmetry were also important in the recent work of ref. 47. We note that the global spin rotation symmetry $SO(3) \subset SO(5)_f$, while the electromagnetic charge symmetry $U(1) \subset SO(5)_b$, and these are the only exact continuous global symmetries of the lattice theory.

We determine the physical interpretation of the B bilinears forming the gauge-neutral $SO(5)_b$ vector and find the following five orders: (*i*)+(*ii*): A d-wave superconductor; this complex order has 2 real components. (*iii*)+(*iv*): Site-charge density waves (stripes) at wavevectors $(\pi, 0)$ and $(0, \pi)$. (*v*): The "d-density wave" (48), which has a staggered pattern of circulating charge currents and breaks time-reversal symmetry. The choice between these orders is made by additional terms allowed by the lattice symmetries which break the $SO(5)_b$ symmetry. With additional dispersion minima, we can obtain charge density waves at other wavevectors, as we discuss in sections 5 and 6.

In the combined theory of the fermionic spinons and bosonic chargons, for the case where the chargon dispersion has two minima, we can now sketch the schematic phase diagram shown in Fig. 2.

For $r > r_c$, the Higgs boson B is massive and can be ignored at low energies, where the theory reduces to $N_f = 2$ massless Dirac fermions coupled to a SU(2) gauge field. The numerical evidence (49–53) indicates that this theory is confining and leads to a phase with $SO(5)_f$ global symmetry broken by either Néel or valence bond solid (VBS) order. For $r < r_c$, the Higgs boson B condenses: This quenches the SU(2) gauge field completely and breaks the $SO(5)_b$ global symmetry, and so, one of the orders listed in the previous paragraph will be present. At half-filling, $r = r_c$ is a possible deconfined critical point (54) described by a conformal field theory with global $SO(5)_f \times SO(5)_b$ symmetry. This CFT is an attractive candidate for describing the transition between the

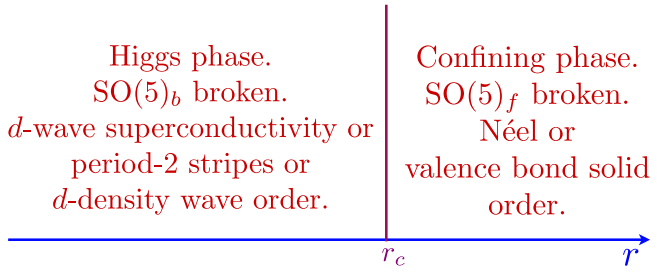

Fig. 2. Schematic phase diagram of the SU(2) gauge theory of fermionic spinons and bosonic chargons discussed in the present paper, for the case where the chargons have only two dispersion minima as in Fig. 3. The SU(2) gauge fluctuations are fully confined in both phases, but the pattern of symmetry breaking is different. The critical point at $r = r_c$ is a possible conformal field theory with $SO(5)_f \times SO(5)_b$ global symmetry.

Néel state and the d-wave superconductor numerically observed by Assaad et al. (55) in the particle–hole symmetric half-filled Hubbard model with an additional square-hopping interaction term.

We conclude this introduction by noting a few of the many earlier works (56) which have considered the interplay of antiferromagnetism, d-wave superconductivity, and charge order in the context of the cuprates, all in a manner distinct from ours; this discussion may be skipped on a first reading.

- Zhang (57) considered a SO(5) symmetry mixing antiferromagnetism and superconductivity. This is not related to our SO(5)s, as antiferromagnetism is part of $SO(5)_f$, while d-wave superconductivity is part of $SO(5)_b$.
- Charge order was obtained in an insulator by the condensation of vortices (58, 59) in the d-wave superconductor.
- A theory for the transition between an easy-plane Néel state (in contrast to the fully SO(3) symmetric Néel order in our case) and a d-wave superconductor without nodal quasiparticles (our d-wave superconductor can have nodal quasiparticles) was obtained (60) in a dual formulation of vortices in both the Néel order and the superconductor.
- A direct transition between the Néel state and the d-wave superconductors was described by Raghu et al. (61) in a weak-coupling analysis of the Hubbard model. It is possible that this transition and that in the quantum Monte Carlo study of Assaad et al. (55) are both described by the deconfined critical theory introduced in the present paper.
- The spin density-wave quantum critical point in a two-dimensional metal was argued to have instabilities to d-wave pairing and charge order with nearly the same strength (62, 63), and theories of the fluctuations of the combined orders have been examined (64–69). There is no fractionalization and no emergent gauge field in these approaches.
- The studies in refs. 70 and 71, closest in spirit to the present study, examined the condensation of chargons from a pseudogap metal described by a $\mathbb{Z}_2$ spin liquid.
- A different fractionalized model for the pseudogap metal was used to study (72, 73) the interplay between spin and charge density wave orders.

1. SU(2) Lattice Gauge Theory for Fermionic Spinons

We begin by recalling the theory for the π-flux spin liquid on the square lattice. Experimental neutron scattering evidence for the relevance of this state to square lattice antiferromagnets was obtained by Dalla Piazza et al. (74) and Headings et al. (75), and numerical evidence by Hering et al. (76). We express the spin operators $\boldsymbol{S_i}$ on site $\boldsymbol{i}$ in terms of fermions $f_{i\alpha}$, where $\alpha = \uparrow, \downarrow$ is spin index, by $\boldsymbol{S_i} = (1/2) f^\dagger_{i\alpha} \boldsymbol{\sigma}_{\alpha\beta} f_{i\beta}$. For spin liquids with an emergent SU(2) gauge field, it is useful to introduce the spinor $\psi_{\boldsymbol{i}}$

$$\psi_{\boldsymbol{i}} = \begin{pmatrix} f_{\boldsymbol{i}\uparrow} \\ f^\dagger_{\boldsymbol{i}\downarrow} \end{pmatrix}, \qquad [1]$$

so that the SU(2) gauge transformation acts as $\psi_{\boldsymbol{i}} \to U_{\boldsymbol{i}} \psi_{\boldsymbol{i}}$, where $U_{\boldsymbol{i}} \in \mathrm{SU}(2)$. We describe the π-flux spin liquid, in the gauge used by ref. 29, by the quadratic fermion Hamiltonian

$$H_f = -iJ \sum_{\langle \boldsymbol{ij} \rangle} \left[\psi^\dagger_{\boldsymbol{i}} e_{\boldsymbol{ij}} U_{\boldsymbol{ij}} \psi_{\boldsymbol{j}} + \boldsymbol{i} \leftrightarrow \boldsymbol{j} \right], \qquad [2]$$

where $\boldsymbol{i,j}$ are nearest neighbors, J is a real coupling constant of order the antiferromagnetic exchange, and $e_{\boldsymbol{ji}} = -e_{\boldsymbol{ij}}$ is a fixed element of the $\mathbb{Z}_2$ center of the gauge SU(2) which ensures π flux per plaquette; we choose

$$e_{\boldsymbol{i},\boldsymbol{i}+\hat{\boldsymbol{x}}} = 1\,, \quad e_{\boldsymbol{i},\boldsymbol{i}+\hat{\boldsymbol{y}}} = (-1)^x, \qquad [3]$$

where $\boldsymbol{i} = (x, y), \hat{\boldsymbol{x}} = (1, 0), \hat{\boldsymbol{y}} = (0, 1)$. The link field $U_{\boldsymbol{ij}} = U^\dagger_{\boldsymbol{ji}}$ is the fluctuating SU(2) lattice gauge field, and the mean-field saddle point of the π-flux phase is obtained by setting $U_{\boldsymbol{ij}} = 1$. We note that the leading i in Eq. **2** is needed to ensure global SU(2) spin-rotation invariance.

At the $U_{\boldsymbol{ij}} = 1$ saddle point, the dispersion of the fermions in H_f has two Dirac nodes at the Fermi level, as shown in Fig. 3.

Linearizing the dispersion at the nodes, we obtain a theory of $N_f = 2$ relativistic, massless Dirac fermions coupled to a SU(2) gauge field. This theory has a global $SO(5)_f$ symmetry (29, 33–37, 77), corresponding to rotations among Néel order and VBS order, which together form a composite order with 5 real components. The Néel-VBS transition has been intensively studied by numerical and bootstrap methods, and the emerging consensus (49–53) is that ground state is ultimately a confining state with $SO(5)_f$ broken: This consensus accounts for the $r > r_c$ portion of the phase diagram in Fig. 2, where the chargons are massive and unimportant at low energies.

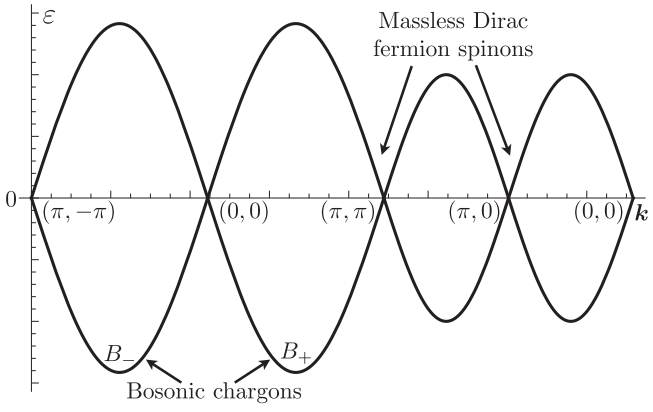

Fig. 3. Common lattice dispersion of the fermionic spinons and bosonic chargons in Eqs. **2** and **8**, for the case in section 3 where the chargons have only two degenerate minima. The boson dispersion is shifted by the constant r in Eq. **11**. The fermion and boson low-energy theories focus on distinct points in the Brillouin zone. The degenerate bosonic chargons $B_\pm$ are at $(\pi/2, \pm\pi/2)$.

2. SU(2) Lattice Gauge Theory for Bosonic Chargons

We introduce a chargon field (13–15)

$$B_{\boldsymbol{i}} \equiv \begin{pmatrix} B_{1\boldsymbol{i}} \\ B_{2\boldsymbol{i}} \end{pmatrix}, \qquad \mathcal{B}_{\boldsymbol{i}} \equiv \begin{pmatrix} B_{1\boldsymbol{i}} & -B^*_{2\boldsymbol{i}} \\ B_{2\boldsymbol{i}} & B^*_{1\boldsymbol{i}} \end{pmatrix}, \qquad [4]$$

on each lattice site, where $B_{1\boldsymbol{i}}$ and $B_{2\boldsymbol{i}}$ are complex boson. We view the chargon as a Higgs field which couples the spinons $\psi_{\boldsymbol{i}}$ to the physical electrons $\bar{c}_{\boldsymbol{i}\alpha}$. For the doped system, the $\bar{c}_{\boldsymbol{i}\alpha}$ annihilates an electron-like quasiparticle near the Fermi surface of the hole pockets; for the undoped system, the $\bar{c}_{\boldsymbol{i}\alpha}$ annihilates an electronic quasiparticle just above the charge gap. After introducing

$$\bar{C}_{\boldsymbol{i}} = \begin{pmatrix} \bar{c}_{\boldsymbol{i}\uparrow} \\ \bar{c}^\dagger_{\boldsymbol{i}\downarrow} \end{pmatrix}, \qquad [5]$$

the coupling between the chargons, electrons, and spinons can be written as

$$\begin{aligned} H_H &= i \sum_{\boldsymbol{i}} \left(\psi^\dagger_{\boldsymbol{i}} \, \mathcal{B}_{\boldsymbol{i}} \, \bar{C}_{\boldsymbol{i}} - \bar{C}^\dagger_{\boldsymbol{i}} \, \mathcal{B}^\dagger_{\boldsymbol{i}} \, \psi_{\boldsymbol{i}} \right) \\ &= i \sum_{\boldsymbol{i}} \left(B_{1\boldsymbol{i}} f^\dagger_{\boldsymbol{i}\alpha} \bar{c}_{\boldsymbol{i}\alpha} - B_{2\boldsymbol{i}} \varepsilon_{\alpha\beta} f_{\boldsymbol{i}\alpha} \bar{c}_{\boldsymbol{i}\beta} \right) + \text{H.c.}, \end{aligned} \qquad [6]$$

where $\varepsilon_{\alpha\beta}$ is the unit antisymmetric tensor. The first line in Eq. **6** makes the invariance under gauge SU(2), global spin SU(2), and global charge U(1) transparent. In particular, we have $B_{\boldsymbol{i}} \to U_{\boldsymbol{i}} B_{\boldsymbol{i}}$ under gauge SU(2), $B_{\boldsymbol{i}} \to e^{i\phi} B_{\boldsymbol{i}}$ under electromagnetic U(1), and $B_{\boldsymbol{i}} \to B_{\boldsymbol{i}}$ under global spin SU(2). An explicit microscopic derivation of the form of H_H can be obtained in the ancilla model (9, 10), as we describe in *SI Appendix*, 1. Here, we regard H_H as the simplest allowed coupling consistent with the gauge and global symmetries.

We now obtain the form of the lattice effective action for $B_{\boldsymbol{i}}$ by requiring invariance under lattice symmetries and time-reversal under the projective transformations of the π-flux phase. The projective transformations of the fermionic spinons f_α have been computed earlier (29), those of the electrons $\bar{c}_\alpha$ must be trivial, and those of the bosonic charges B then follow from the invariance of Eq. **6**. The transformations are listed in Table 1.

The key property is the relation

$$T_x T_y = -T_y T_x, \qquad [7]$$

which ensures π-flux on both spinons and chargons and at least two degenerate minima for the chargons.

Table 1. Projective transformations of the *f* spinons and *B* chargons on lattice sites $\boldsymbol{i} = (\boldsymbol{x}, \boldsymbol{y})$ under the symmetries $\boldsymbol{T_x} : (\boldsymbol{x}, \boldsymbol{y}) \to (\boldsymbol{x}+\boldsymbol{1}, \boldsymbol{y})$; $\boldsymbol{T_y} : (\boldsymbol{x}, \boldsymbol{y}) \to (\boldsymbol{x}, \boldsymbol{y}+\boldsymbol{1})$; $\boldsymbol{P_x} : (\boldsymbol{x}, \boldsymbol{y}) \to (-\boldsymbol{x}, \boldsymbol{y})$; $\boldsymbol{P_y} : (\boldsymbol{x}, \boldsymbol{y}) \to (\boldsymbol{x}, -\boldsymbol{y})$; $\boldsymbol{P_{xy}} : (\boldsymbol{x}, \boldsymbol{y}) \to (\boldsymbol{y}, \boldsymbol{x})$; and time-reversal $\mathcal{T}$

Symmetry	f_α	B_a
T_x	$(-1)^y f_\alpha$	$(-1)^y B_a$
T_y	f_α	B_a
P_x	$(-1)^x f_\alpha$	$(-1)^x B_a$
P_y	$(-1)^y f_\alpha$	$(-1)^y B_a$
P_{xy}	$(-1)^{xy} f_\alpha$	$(-1)^{xy} B_a$
$\mathcal{T}$	$(-1)^{x+y} \varepsilon_{\alpha\beta} f_\beta$	$(-1)^{x+y} B_a$

The indices α, β refer to global SU(2) spin, while the index $a = 1, 2$ refers to gauge SU(2).

With the transformations in Table 1 in hand, we write down the most general effective Lagrangian for the $B_{\boldsymbol{i}}$, keeping only terms quadratic and quartic in the $B_{\boldsymbol{i}}$, and with only on-site or nearest-neighbor couplings. In this manner, we obtain the Lagrangian (terms with time derivatives will be considered in Section 7)

$$\mathcal{L}(B) = r \sum_{\boldsymbol{i}} B^\dagger_{\boldsymbol{i}} B_{\boldsymbol{i}} - i w_1 \sum_{\langle \boldsymbol{ij} \rangle} \left[B^\dagger_{\boldsymbol{i}} e_{\boldsymbol{ij}} U_{\boldsymbol{ij}} B_{\boldsymbol{j}} + \boldsymbol{i} \leftrightarrow \boldsymbol{j} \right] + \mathcal{V}(B), \qquad [8]$$

where r, w_1 are real Landau parameters, and the quartic terms are in $\mathcal{V}(B)$. The hopping terms in Eq. **8** are identical to the hopping terms for the fermionic spinons in Eq. **2**. However, there is a "mass" term, r, present for the chargons, which was not allowed for the spinons—we will use r as the tuning parameter across the transition in which the B condense, as in Fig. 2.

The quartic interaction terms in $\mathcal{V}(B)$ are more conveniently expressed in terms of quadratic gauge invariant observables. By examining the transformations in Table 1, we can deduce the following correspondences between bilinears of the B with those of the bilinears of the gauge-neutral electrons (*SI Appendix*, 1 for the difference between the renormalized quasiparticle operator $\bar{c}_\alpha$ and bare electron c_α):

$$\begin{aligned} &\text{site charge density: } \left\langle c^\dagger_{\boldsymbol{i}\alpha} c_{\boldsymbol{i}\alpha} \right\rangle \sim \rho_{\boldsymbol{i}} = B^\dagger_{\boldsymbol{i}} B_{\boldsymbol{i}} \\ &\text{bond density: } \left\langle c^\dagger_{\boldsymbol{i}\alpha} c_{\boldsymbol{j}\alpha} + c^\dagger_{\boldsymbol{j}\alpha} c_{\boldsymbol{i}\alpha} \right\rangle \\ &\qquad\qquad \sim Q_{\boldsymbol{ij}} = Q_{\boldsymbol{ji}} = \text{Im} \left(B^\dagger_{\boldsymbol{i}} e_{\boldsymbol{ij}} U_{\boldsymbol{ij}} B_{\boldsymbol{j}} \right) \\ &\text{bond current: } i \left\langle c^\dagger_{\boldsymbol{i}\alpha} c_{\boldsymbol{j}\alpha} - c^\dagger_{\boldsymbol{j}\alpha} c_{\boldsymbol{i}\alpha} \right\rangle \\ &\qquad\qquad \sim J_{\boldsymbol{ij}} = -J_{\boldsymbol{ji}} = \text{Re} \left(B^\dagger_{\boldsymbol{i}} e_{\boldsymbol{ij}} U_{\boldsymbol{ij}} B_{\boldsymbol{j}} \right) \\ &\text{Pairing: } \left\langle \varepsilon_{\alpha\beta} c_{\boldsymbol{i}\alpha} c_{\boldsymbol{j}\beta} \right\rangle \sim \Delta_{\boldsymbol{ij}} = \Delta_{\boldsymbol{ji}} = \varepsilon_{ab} B_{a\boldsymbol{i}} e_{\boldsymbol{ij}} U_{\boldsymbol{ij}} B_{b\boldsymbol{j}}. \end{aligned} \qquad [9]$$

We have checked the correspondences in Eq. **9** in a few cases by computing the expectation values of the c_α bilinears in the ancilla theory presented in *SI Appendix*, 1 and comparing them to the values of B bilinears. Now, we can write an expression for $\mathcal{V}(B)$ by keeping all quartic terms which involve nearest-neighbor sites:

$$\begin{aligned} \mathcal{V}(B) = &\frac{u}{2} \sum_{\boldsymbol{i}} \rho^2_{\boldsymbol{i}} + V_1 \sum_{\boldsymbol{i}} \rho_{\boldsymbol{i}} \left(\rho_{\boldsymbol{i}+\hat{\boldsymbol{x}}} + \rho_{\boldsymbol{i}+\hat{\boldsymbol{y}}} \right) + g \sum_{\langle \boldsymbol{ij} \rangle} \left| \Delta_{\boldsymbol{ij}} \right|^2 \\ &+ J_1 \sum_{\langle \boldsymbol{ij} \rangle} Q^2_{\boldsymbol{ij}} + K_1 \sum_{\langle \boldsymbol{ij} \rangle} J^2_{\boldsymbol{ij}}. \end{aligned} \qquad [10]$$

3. Low-Energy Continuum Theory of Chargons with Two Dispersion Minima

The quadratic form of the chargons in Eq. **8** is identical to that for the spinons in Eq. **2**, and so, the dispersion of the chargons is also that shown in Fig. 3. In the low-energy theory for the fermionic spinons, we had to focus on the nodal points in the Brillouin zone at the Fermi level. In contrast, for the bosonic chargons, we have to focus on the minima of the same dispersion. These are at distinct points in the Brillouin zone, and this is a factor in the distinct lattice symmetries of the orders described by the chargons.

Specifically, the dispersion of chargons is

$$\varepsilon(\boldsymbol{k}) = r \pm 2|w_1| \sqrt{\sin^2 k_x + \sin^2 k_y}, \qquad [11]$$

Table 2. As in Table 1, but for the continuum fields of Section 3

Symmetry	B_{a+}	B_{a-}
T_x	$-iB_{a-}$	$-iB_{a+}$
T_y	$-iB_{a+}$	iB_{a-}
P_x	B_{a+}	B_{a-}
P_y	B_{a+}	B_{a-}
P_{xy}	$-(B_{a+}+B_{a-})/\sqrt{2}$	$-(B_{a+}-B_{a-})/\sqrt{2}$
$\mathcal{T}$	B_{a+}	B_{a-}

and the band minima are at $\boldsymbol{Q}_+ = \frac{\pi}{2}(1,1)$ and $\boldsymbol{Q}_- = \frac{\pi}{2}(1,-1)$. We can expand the B in terms of the eigenmodes at the minima using fields B_{as} ($a = 1, 2$ is the gauge SU(2) index, and $s = \pm$ refers to the band minima)

$$B_a(\boldsymbol{r}) = \begin{cases} -B_{a+}e^{i\pi(x+y)/2} + B_{a-}(\sqrt{2}+1)e^{i\pi(x-y)/2}, \\ x \text{ even} \\ B_{a+}(\sqrt{2}+1)e^{i\pi(x+y)/2} - B_{a-}e^{i\pi(x-y)/2}, \\ x \text{ odd} \end{cases} \quad [12]$$

This expansion leads to the symmetry transformations in Table 2, which follow from the transformations in Table 1.

Obtaining the action of P_{xy} is a little involved, and it is obtained by requiring

$$-B_{a+} + B_{a-}(\sqrt{2}+1) \to -B_{a+} + B_{a-}(\sqrt{2}+1), \quad \text{for } x \text{ even}, y \text{ even}$$
$$B_{a+}(\sqrt{2}+1) + B_{a-} \to -B_{a+}(\sqrt{2}+1) - B_{a-}, \quad \text{for } x \text{ odd}, y \text{ odd},$$

and also similar relations when x and y have opposite parity. The relation in Eq. **7** continues to hold in Table 2.

We now define the following gauge-invariant order parameters

$$\begin{aligned} x-\text{CDW}: &\quad \rho_{(\pi,0)} = B^*_{a+}B_{a+} - B^*_{a-}B_{a-} \\ y-\text{CDW}: &\quad \rho_{(0,\pi)} = B^*_{a+}B_{a-} + B^*_{a-}B_{a+} \\ d-\text{density wave}: &\quad D = i\left(B^*_{a+}B_{a-} - B^*_{a-}B_{a+}\right) \\ d-\text{wave superconductor}: &\quad \Delta = \varepsilon_{ab}B_{a+}B_{b-}, \end{aligned} \quad [13]$$

The transformations of these expressions in Table 3 identify them as the labeled orders.

Note that T_x and T_y commute for these gauge-invariant order parameters, and Eq. **7** does not apply to Table 3.

Table 3. As in Table 1, but for the order parameters of Section 3

Symmetry	$\rho_{(\pi,0)}$	$\rho_{(0,\pi)}$	D	Δ
T_x	$-\rho_{(\pi,0)}$	$\rho_{(0,\pi)}$	$-D$	Δ
T_y	$\rho_{(\pi,0)}$	$-\rho_{(0,\pi)}$	$-D$	Δ
P_x	$\rho_{(\pi,0)}$	$\rho_{(0,\pi)}$	D	Δ
P_y	$\rho_{(\pi,0)}$	$\rho_{(0,\pi)}$	D	Δ
P_{xy}	$\rho_{(0,\pi)}$	$\rho_{(\pi,0)}$	$-D$	$-\Delta$
$\mathcal{T}$	$\rho_{(\pi,0)}$	$\rho_{(0,\pi)}$	$-D$	Δ

Table 4. Representative ansatzes for the phases

B_{a+}	B_{a-}	$\rho_{(\pi,0)}$	$\rho_{(0,\pi)}$	D	Δ
$(b,0)$	$(0,0)$	$\lvert b\rvert^2$	0	0	0
$(b,0)/\sqrt{2}$	$(b,0)/\sqrt{2}$	0	$\lvert b\rvert^2$	0	0
$(b,0)/\sqrt{2}$	$(-ib,0)/\sqrt{2}$	0	0	$\lvert b\rvert^2$	0
$(b,0)$	$(0,b)$	0	0	0	b^2

We can now write down the Landau potential in this continuum limit

$$V(B_{as}) = r\,B^*_{as}B_{as} + u\,(B^*_{as}B_{as})^2 + v_1\left[\rho_{(\pi,0)}\right]^2 + v_1\left[\rho_{(0,\pi)}\right]^2 + v_2\,D^2 + v_3|\Delta|^2. \quad [14]$$

At $v_{1,2,3} = 0$, this Higgs potential has an enhanced symmetry also present in the terms displayed in Eq. **8**: There is a SO(8) symmetry of rotations among the 8 real components of B_{as}. After including the coupling to the SU(2) gauge field, we must factor out a SO(3) subgroup, which leaves the advertised $SO(5)_b$ symmetry for gauge-invariant order parameters. Indeed, we can now verify that the order parameters in Eq. **13** do indeed correspond to a 5-component order parameter which rotates under $SO(5)_b$, after decomposing Δ into two 2 real components.

We numerically minimized Eq. **14** for nonzero $v_{1,2,3}$ and found only solutions which are either some linear combination of the two CDWs, a d-density wave, or a d-wave superconductor, with no coexistence between different orders. Simple ansatzes for these solutions are shown in Table 4. From these ansatzes, we can immediately determine the phase diagram of Eq. **14**. The Higgs potential is stable provided all $|v_i| < u$, and the lowest energy state is that associated with the smallest of the v_i, i.e., for $v_1 < v_{2,3}$, the lowest energy state is any linear combination of the x-CDW and y-CDW; for $v_2 < v_{1,3}$, we obtain the d-density wave with broken time-reversal symmetry, and for $v_3 < v_{1,2}$, we have a d-wave superconductor. The nature of the nodal Bogoliubov excitations of this superconductor will be similar to that studied in ref. 71.

4. Chargon Lattice-Mean-Field Theory with Nearest-Neighbor Couplings

In this section, we present the results of numerically minimizing the lattice potential for the chargons in Eqs. **8** and **10** on an 8×8 real space lattice. As there are a large number of parameters to minimize over, we will show results for regions of parameter space where the most general states can be found by varying only 2 parameters.

Fig. 4 shows the agreement between the continuum and lattice phase diagrams when the lattice parameters are specifically chosen to reproduce the continuum free energy parameters in the low-energy limit as described in *SI Appendix*, 4. We also choose r to lie near the band minima.

In this case, in agreement with analytical expectations, we find that lattice parameters corresponding to $v_2 < v_1$ and $v_2 < 0$ lead to a d-density wave state. This state breaks time-reversal symmetry and is characterized by a circulating current pattern as shown in Fig. 4. For $v_1 < v_2$ and $v_1 < 0$, we find, exactly as in the continuum theory, that any linear combination of CDW order at $(0,\pi)$ and $(\pi,0)$ is favored. For $v_1 > 0$ and $v_2 > 0$, we find a d-wave superconductor appears where the precise phase boundaries are determined by u and g in Eq. **10**. We have verified

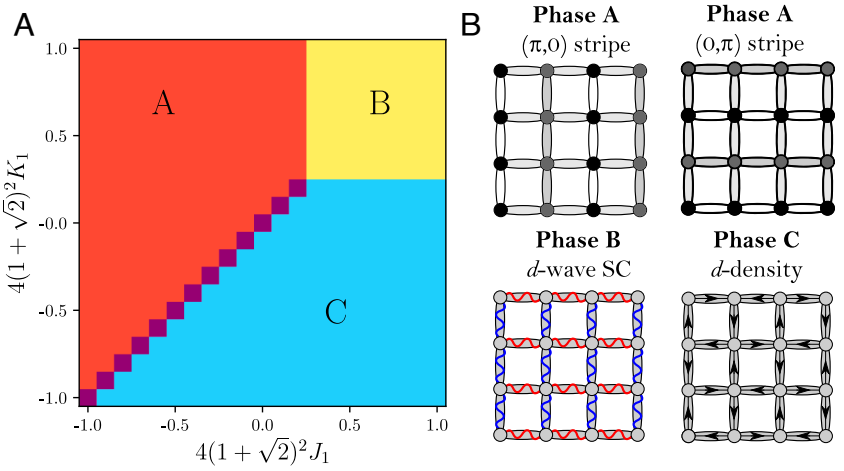

Fig. 4. Mean-field analysis of the lattice model of chargons in the regime where the continuum theory with two minima applies. (*A*) shows the phase diagram as a function of lattice parameters J_1 and K_1, while simultaneously varying V_1 such that $(V_1 + J_1)c_0 = 4$, $c_0 = 4(1+\sqrt{2})^2$. Then, taking the continuum limit leads to $v_1 = c_0 J_1$, $v_2 = c_0 K_1$, and $u = 4$ in Eq. **14** as explained in *SI Appendix*, 4. We here further assume $w < 0$ and $g > 0$. We obtain three different types of phases, exactly as in the continuum theory: a continuous set (A) of degenerate CDW states given by an arbitrary superposition of density modulations with wavevectors $(\pi, 0)$, $(0, \pi)$, a *d*-wave superconductor (B), and a *d*-density wave (C). These phases are illustrated on the square lattice in (B), where the shading indicates the on-site and bond densities, black arrows the currents, and the blue/red wiggly lines nearest-neighbor pairing with positive/negative amplitude.

in these cases that the forms for B_i in our solutions obey Eq. **12** to a very good approximation.

We next present a more general phase diagram, with parameters in the lattice model, Eqs. **8** and **10**, chosen to be far from the limit where the continuum model applies. To capture a large variety of different ground states, we study both $g < 0$ and $g > 0$ with phase diagrams shown in Fig. 5 *A* and *B*, respectively, where we further choose a negative J_1 and positive value of u in Eq. **10** for stability. Besides the *d*-density wave and the *d*-wave superconductor already present in Fig. 4, we also find a CDW with ordering wave vector (π, π), which coexists with either a *d*-density wave or superconductivity; furthermore, the previous degeneracy of any superposition of *x*-CDW and *y*-CDW is lifted; depending on V_1, we either find a unidirectional 2-site stripe state or a bidirectional CDW, which preserves the four-fold rotational symmetry of the lattice. These additional states are illustrated in Fig. 5*C*. In future work, it would be interesting to study whether this coexistence of multiple orders survives the inclusion of SU(2) gauge fluctuations.

5. Low-Energy Continuum Theory of Chargons with More Than Two Dispersion Minima

When longer-range hoppings of chargons are present, the dispersion can in general have multiple minima. The strategy here is similar to that followed in ref. 78 for the confinement transition out of a $\mathbb{Z}_2$ spin-liquid model of the pseudogap by condensation of vison. *SI Appendix*, 2 describes the general structure of the hopping terms in our present SU(2) gauge theory which are compatible with Table 1. The shortest-ranged terms are

$$\begin{aligned} F_0(B) = \sum_{\boldsymbol{i}} \Big\{ & \frac{r}{2} B_{\boldsymbol{i}}^\dagger B_{\boldsymbol{i}} - w_2 (B_{\boldsymbol{i}}^\dagger B_{\boldsymbol{i}+2\hat{\boldsymbol{x}}} + B_{\boldsymbol{i}}^\dagger B_{\boldsymbol{i}+2\hat{\boldsymbol{y}}}) \\ & - i w_1 \left[B_{\boldsymbol{i}}^\dagger B_{\boldsymbol{i}+\hat{\boldsymbol{x}}} + (-1)^x B_{\boldsymbol{i}}^\dagger B_{\boldsymbol{i}+\hat{\boldsymbol{y}}} \right] \\ & - i w_3 \left[(-1)^x B_{\boldsymbol{i}}^\dagger B_{\boldsymbol{i}+2\hat{\boldsymbol{x}}+\hat{\boldsymbol{y}}} - (-1)^x B_{\boldsymbol{i}}^\dagger B_{\boldsymbol{i}+2\hat{\boldsymbol{x}}-\hat{\boldsymbol{y}}} \right. \\ & \left. + B_{\boldsymbol{i}}^\dagger B_{\boldsymbol{i}+2\hat{\boldsymbol{y}}+\hat{\boldsymbol{x}}} - B_{\boldsymbol{i}}^\dagger B_{\boldsymbol{i}+2\hat{\boldsymbol{y}}-\hat{\boldsymbol{x}}} \right] \Big\} + \text{h.c.}, \end{aligned} \quad [15]$$

where w_1, w_2, w_3 are real parameters. Choosing a unit cell containing two neighboring sites separated in the *x*-direction, the free energy density in momentum space is

$$\begin{aligned} \mathcal{F}_0(\boldsymbol{k}) = & \left[r - 2w_2 \cos(2k_x) - 2w_2 \cos(2k_y) \right] \mathbb{1} \\ & + \left[2w_1 + 4w_3 \cos(2k_y) \right] \sin(k_x) \tau^x \\ & + \left[2w_1 + 4w_3 \cos(2k_x) \right] \sin(k_y) \tau^z, \end{aligned} \quad [16]$$

where τ^i acts in the sublattice space. The example dispersions associated with Eq. **16** are plotted in *SI Appendix*, Fig. S2 in Appendix 2. When only w_1 is present, the minima are at $\boldsymbol{Q}_\pm$. Adding a finite w_2, the dispersion becomes

$$\begin{aligned} \varepsilon_2(\boldsymbol{k}) &= r - |w_1| \sqrt{4 - 2f(\boldsymbol{k})} - 2w_2 f(\boldsymbol{k}), \\ f(\boldsymbol{k}) &\equiv \cos(2k_x) + \cos(2k_y). \end{aligned} \quad [17]$$

When $w_2 < 0$, the positions of the minima remain at $\boldsymbol{Q}_\pm$. When $w_2 > 0$, the minimum has a ring degeneracy since the energy depends only on $f(\boldsymbol{k})$. When $w_2 > w_1/4\sqrt{2} \approx 0.177 w_1$, the minima begin to expand from the two points $\boldsymbol{Q}_\pm$ (or $f(\boldsymbol{k}) = -2$) to rings around these points. Upon further increasing w_2, the rings will grow and touch when $w_2 = w_1/4 = 0.25 w_1$ (or $f(\boldsymbol{k}) = 0$) and merge to become new rings centered around $(0, 0)$ and $(0, \pi)$. Then, when w_2 dominates, the new rings will shrink until they become points.

When w_3 is further added, the dispersion relation is complicated. Each ring can split into four minima in axial or diagonal directions, corresponding to the cases of $w_3 > 0$ and $w_3 < 0$, respectively. We will focus on the axial splitting case and for concreteness consider an infinitesimal w_3 to split the ring in the regime of $|w_2| \gtrapprox |w_1|/4\sqrt{2}$.

The new incommensurate minima are at

$$\begin{aligned} \boldsymbol{Q}_{+,R/L} &= \left(\frac{\pi}{2} \pm q, \frac{\pi}{2} \right), \ \boldsymbol{Q}_{+T/B} = \left(\frac{\pi}{2}, \frac{\pi}{2} \pm q \right), \\ \boldsymbol{Q}_{-,R/L} &= \left(\frac{\pi}{2} \pm q, -\frac{\pi}{2} \right), \ \boldsymbol{Q}_{+T/B} = \left(\frac{\pi}{2}, -\frac{\pi}{2} \pm q \right), \end{aligned} \quad [18]$$

where the *T, B, L,* and *R* stand for *Top*, *Bottom*, *Left*, and *Right*, respectively, and q is a number depending on r, w_1, w_2, and w_3.

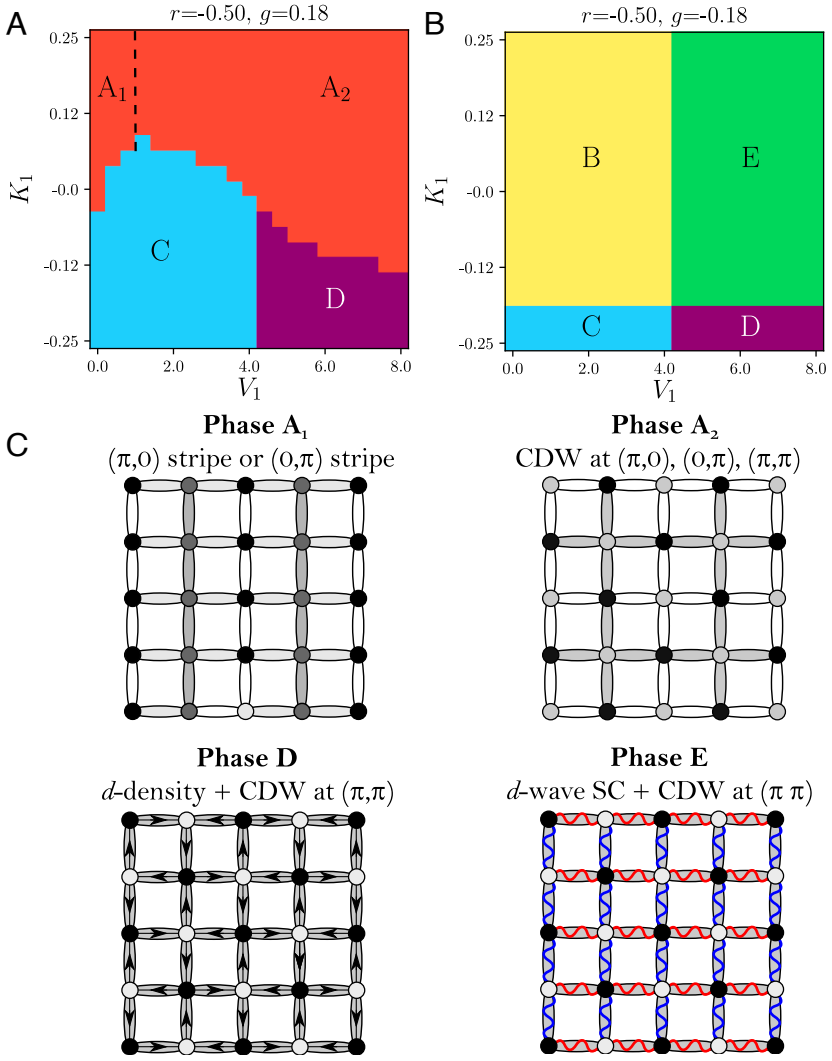

Fig. 5. Phases of lattice chargon theory away from the continuum limit. Phase diagrams as a function of V_1 and K_1 at fixed $J_1 = -0.15$, $u = 2.4$, and $r = -0.5$ are shown for (*A*) positive and (*B*) negative g. Phases B and C are the same as in Fig. 4, whereas A splits into a unidirectional, nematic stripe state (A_1) and a bidirectional, nonnematic (A_2) state. There are additional phases—a *d*-density wave state (D) and a *d*-wave superconductor (E) both coexisting with a bidirectional CDW at (π, π).

We expand the boson fields in terms of eigenmodes at the 8 minima,

$$B(\boldsymbol{r}) = -\sum_{\alpha} \left[e^{i\boldsymbol{Q}_{+\alpha}\cdot\boldsymbol{r}} \begin{pmatrix} 1 \\ v_\alpha \end{pmatrix} B_{+\alpha} + e^{i\boldsymbol{Q}_{-\alpha}\cdot\boldsymbol{r}} \begin{pmatrix} v_\alpha \\ 1 \end{pmatrix} B_{-\alpha} \right]. \quad [19]$$

Here, the summation runs over $\alpha \in \{L, R, T, B\}$, v_α is a complicated real function of q and thus the parameters r, w_1, w_2, w_3. There is only one independent v_α: The v_α satisfy $v_L = v_R$, $v_T = v_B$, and $(1+v_T)(1+v_B) = 2$. When $q \to 0$, the expression Eq. **19** reduces to Eq. **12**. The symmetry transformations of the low-energy fields in Eq. **19**, the expressions for the gauge-invariant order parameters in terms of these fields, and the allowed quartic terms in the chargon free energy are all discussed in *SI Appendix*, 2.

Here, we write down ansatzes for a few interesting states, along the lines of Table 4 for the commensurate case. Only the nonzero values of $B_{as\alpha}$ and order parameters are shown.

- x-CDW: $B_{a+R} = (b_1, 0)$, $B_{a+L} = (b_2, 0)$, $\rho_{(n\pi+2q,0)} \propto b_2^* b_1$, $\rho_{(n\pi-2q,0)} = b_1^* b_2$, $\rho_{(n\pi,0)} \propto |b_1|^2 + |b_2|^2$. Here $n = 0, 1$.
- y-CDW: $B_{a+T} = (b_1, 0)/\sqrt{2}$, $B_{a-T} = (b_1, 0)/\sqrt{2}$, $B_{a+B} = (b_2, 0)/\sqrt{2}$, $B_{a-B} = (b_2, 0)/\sqrt{2}$, $\rho_{(0,n\pi+2q)} = b_2^* b_1$, $\rho_{(0,n\pi-2q)} \propto b_1^* b_2$, $\rho_{(0,n\pi)} \propto |b_1|^2 + |b_2|^2$.
- x-CDW and dDW: $B_{a+R} = (b, 0)/\sqrt{2}$, $B_{a-R} = (b, 0)/\sqrt{2}$, $B_{a+L} = (b, 0)/\sqrt{2}$, $B_{a-L}/\sqrt{2} = (-b, 0)$, $\rho_{(n\pi+2q,0)} = |b|^2$, $\rho_{(n\pi-2q,0)} \propto |b|^2$, $D \propto -2|b|^2 \sin(2qx)$.
- d-wave superconductor: $B_{a+R} = (b, 0)$, $B_{a-L} = (0, b)$, $\Delta \propto b^2$, $\rho_{(0,0)} \propto 2|b|^2$.
- Pair density wave: $B_{a+R} = (b_1, 0)$, $B_{a-R} = (0, b_1)$, $B_{a+L} = (b_2, 0)$, $B_{a-L} = (0, b_2)$, $\Delta \propto 2b_1 b_2 + b_1^2 e^{2iqx} + b_2^2 e^{-2iqx}$, $\rho \propto 2|b_1|^2 + 2|b_2|^2 + 2b_1^* b_2 e^{2iqx} + 2b_2^* b_1 e^{-2iqx}$.

Note that a spatially uniform d-wave superconductor remains a possible solution even when we include only fields at the incommensurate points in Eq. **19**. However, we have been unable to find a solution which is a pure incommensurate charge density wave at wavevectors, say, $(\pi \pm 2q)$. In the examples shown above, there is either an additional charge density wave at $(\pi, 0)$ or a d-density wave. However, a pure commensurate charge density wave does exist, e.g., at $(\pi/2, 0)$, for then $(\pi, 0)$ is an allowed harmonic.

6. Chargon Lattice-Mean-Field Theory with Further-Neighbor Couplings

In this section, we will describe additional charge-ordered phases which emerge when we include quartic couplings beyond the nearest neighbor in Eq. **10**. More specifically, we will add

$$\mathcal{V}_{\rm add}(B) = \sum_{a,b} V_{a,b} \sum_{\mathbf{i}} \rho_{\mathbf{i}} \rho_{\mathbf{i}+a\hat{\mathbf{x}}+b\hat{\mathbf{y}}}, \qquad [20]$$

with $V_{a,b} = V_{b,a} = V_{a,-b} = V_{-a,b}$ to $\mathcal{V}(B)$ but will not include the further-neighbor terms $w_{2,3}$ quadratic in $B_{\boldsymbol{i}}$ which were already studied in the previous section. As we will see below, this is sufficient to stabilize stripe states with 4-site periodicity and, thus, connect our analysis to the period-4 stripe states found in cuprate experiments (79).

Exploring all of parameter space of couplings $V_{a,b}$ is not practical, and so, we will restrict ourselves to just a few additional nonzero couplings out to fourth-nearest neighbors. We find that setting all $V_{a,b}$, including $V_{1,0} = V_{0,1} = V_1$, to zero except for $V_{2,2}$, $V_{2,-2}$, $V_{1,1}$, and $V_{1,-1}$ stabilizes period-4 stripe states, as summarized in Fig. 6. We find two types of period-4 stripe states; see Fig. 6*B*; the first (phase F) is centered on the bonds and coexists with current order with strength which modulates with the density. The second is a site-centered period-4 stripe state which may (phase G) coexist with current order that modulates with the density or appears without any additional current order (phase H). We note a small region (not shown in Fig. 6) at the phase boundary between phases H and G where another state appears with an additional 2-site charge modulation along the y (x) direction with much smaller magnitude compared to the primary period-4 modulation along x (y). Due to the smallness of this additional symmetry breaking compared to the part of this state which is identical to G, we do not separately denote this state on our phase diagram. We also find a region of pure d-density wave for small $V_{2,2}$ and small $V_{1,1}$ and a region of period 2 unidirectional stripe state for small $V_{2,2}$ and large $V_{1,1}$. We note that these orderings are all obtained within the chargon mean field theory, and it would be interesting to study their fate after including SU(2) gauge fluctuations.

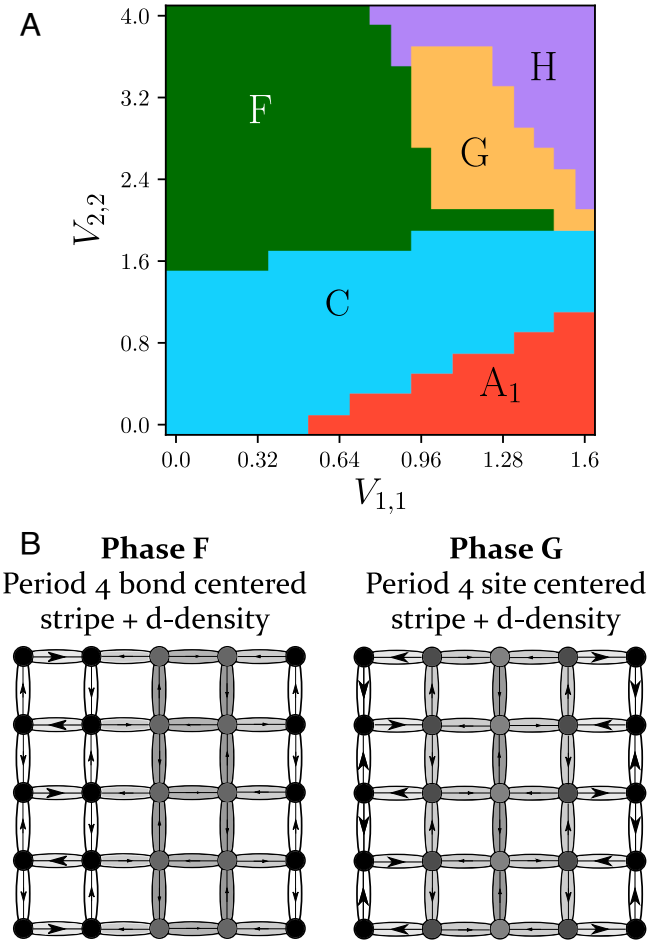

Fig. 6. We show (*A*) the phase diagram of the chargon lattice theory as a function of additional further-neighbor density-density quartic terms, Eq. **20**, which stabilize various types of charge-modulated states. We take $u = 2.4$, $w = 0.5$, $J_1 = 0.2$, $K_1 = 0.25$, and $g = 0.3$. We distinguish between a CDW which orders only at wave vectors $(\pi/2, 0)$ and $(0, \pi/2)$ (phase F) and a stripe state which orders at $(\pi/2, 0)$, $(0, \pi/2)$, $(0, \pi)$, and $(\pi, 0)$ (phase H or G if coexisting with d-density wave), d-density wave order (C), and a period-2 stripe state (A_1). We show what the charge and bond density look like for phase F (*B*, *Left*) and for G (*B*, *Right*). Both are period-4 stripe states, and both have additional currents which modulate spatially.

7. Combined SU(2) Gauge Theory

Let us now collect all the terms in our SU(2) gauge theory for the underdoped cuprates:

- H_f in Eq. **2** describes the fermionic spinons transforming as a fundamental of SU(2)
- The chargon Higgs sector is described by $\mathcal{L}(B)$ in Eq. **8**, along with additional longer-range terms discussed in Sections 5 and 6. The chargon Higgs also transforms as a fundamental of SU(2).
- The hole pockets in the nodal region of the Brillouin zone are described by H_{cg} in *SI Appendix*, Eq. S1 in SI Appendix 1.
- All the above sectors are coupled by Higgs-fermion coupling H_H in Eq. **6**, or more specifically by H_{fg} in *SI Appendix*, Eq. S2 in SI Appendix 1.

The remarkable similarity of the above structure to the Weinberg-Salam SU(2)×U(1) gauge theory of weak interactions (80) may already have been noticed by the alert reader. The electromagnetic U(1) is treated as effectively global in our case, the spinons map to the neutrinos, the electrons and chargons map to the electrons and Higgs bosons, and fermions and bosons are all coupled via the simplest gauge-invariant Yukawa coupling as in Eq. **6**.

In *SI Appendix*, 3, we integrate out the fermions and obtain an effective action for chargons. In addition to the terms just summarized above, this leads to terms with time derivatives of B. In general, a linear-time derivative term $B^\dagger \partial_\tau B$ is allowed, and this will spoil explicit relativistic invariance. However, it remains possible that the $B^\dagger \partial_\tau B$ term is irrelevant at strongly coupled fixed points which describes a quantum phase transition. With particle–hole symmetry in the c_α electron band-structure, the $B^\dagger \partial_\tau B$ term is absent. We also note that in the low-energy limit of section 2, the $B_s^\dagger \partial_\tau B_s$ term has a global symmetry which is smaller than $SO(5)_b$, but $|\partial_\tau B_s|^2$ does have the full $SO(5)_b$ symmetry.

At half-filling, when c_α spectrum is gapped, this procedure of integrating out the c_α is safe. Assuming particle–hole symmetry, and only two minima in the chargon dispersion, we obtain a relativistic theory for $N_f = 2$ massless Dirac fermions Ψ, and $N_b = 2$ scalars B_s ($s = \pm$) both coupled minimally to a SU(2) gauge field with Lagrangian

$$\mathcal{L} = i\overline{\Psi}\gamma_\mu D_\mu \Psi + |D_\mu B_s|^2 + V(B_s), \qquad [21]$$

where the scalar potential V is specified in Eq. **14**, γ_μ are the Dirac matrices, and D_μ is a covariant derivative. At $v_{1,2,3} = 0$,

this theory is explicitly invariant under an $SO(5)_f \times SO(5)_b$ global symmetry, which leads to our proposal of a conformal field theory at the $r = r_c$ critical point in Fig. 2. We propose this CFT as a description of the phase transition between the antiferromagnet and the d-wave superconductor found in the weak-coupling repulsive Hubbard model by Raghu et al. (61), perhaps extended to strong coupling with additional antiferromagnetic exchange interactions. Depending on the fate of the $v_{1,2,3}$ couplings, as well as possible quartic boson-fermions couplings, there could also be fixed points with a smaller global symmetry. We leave a careful examination of such terms to future work.

We also note the study of refs. 81–83 which proposed and obtained numerical evidence for a CFT with a SU(2) gauge field and the same fermionic content as Eq. **21**, but with Higgs bosons which were adjoints (and not fundamentals) of SU(2). This CFT described a deconfined critical point between an antiferromagnet and an "orthogonal semimetal" with the topological order of a $\mathbb{Z}_2$ spin liquid.

8. Discussion

The π-flux state with fermionic spinons (28) is one of the earliest versions of a resonating valence bond spin liquid on the square lattice. It was realized early on that fluctuations about this mean-field state are described by a SU(2) gauge theory (13, 14, 31, 32). Furthermore, early work also recognized that doping such a spin-liquid state led naturally to a d-wave superconductor (13, 15, 31, 39–43). This connection is supported by recent numerical evidence (84), for d-wave superconductivity in doped antiferromagnets near the Néel-VBS transition, given the relationship between the π-flux spin liquid and the Néel-VBS transition (85).

Here, we have investigated the consequences of a basic feature of the π-flux spin liquid to d-wave superconductor transition (this feature does not apply to the "staggered flux" spin liquid used elsewhere (13–15); *SI Appendix*, 5). This transition is also a confinement transition of the SU(2) gauge field of the spin liquid. By Higgs-confinement continuity (86), the transition can be implemented by the condensation of a Higgs field which transforms as a fundamental of SU(2). For the confining phase to be a superconductor, the Higgs field must also carry an electromagnetic charge, and these requirements lead essentially uniquely to the Higgs field being the bosonic chargon B (13–15). The basic feature is that the chargon B must also experience π-flux—this follows from the fact that the electron, which is a gauge-invariant combination of the spinon and the chargon, cannot experience any flux of the SU(2) gauge field. In the presence of a π-flux, the chargon dispersion is required (46) to have at least a twofold degeneracy in its low-energy spectrum. By exploiting this degeneracy, we have shown that a variety of competing charge-ordered states also appear naturally as the outcomes of the confinement of the π-flux spin liquid.

The minimal SU(2) lattice gauge theory of the spinons and chargons is given by Eqs. **2** and **8**, supplemented by the time-derivative terms discussed in *SI Appendix*, 3. Longer-range terms discussed in sections 5 and 6 can also be included. The phase diagrams in sections 4 and 6 were obtained in a mean-field treatment, in which we set the SU(2) gauge field $U_{ij} = 1$, and treated B_i as spatially varying complex numbers to be optimized. Closer connections to the cuprate phase diagram require a more complete treatment of the SU(2) gauge fluctuations: We hope that such lattice gauge theory simulations will be carried out. The theory of just the chargons and spinons, and only the second-order time-derivative term in B (*SI Appendix*, 3), has no sign-problem, and determining its phase diagram will shed considerable light on the cuprate phase diagram. The phases in Figs. 5 and 6 have coexisting broken symmetries which are not required by any conventional symmetry principles and are instead a consequence of the use of a mean-field fractionalized order parameter B. It would be interesting to see whether this coexistence is present in a complete theory which includes SU(2) gauge fluctuations.

After the onset of SU(2) confinement at low temperatures along arrow $\mathbb{A}$ in Fig. 1, it is possible that an effective theory involving only the competing superconducting and charge orders (64–69) will become applicable. However, at higher temperatures, there must be a change to the deconfined characteristics of the pseudogap metal, and the theory presented here is designed to address this transformation. Such a theory also points to resolutions of the key puzzles noted in the introduction:

1. The FL* state with an underlying π-flux spin liquid can fit the photoemission data in the pseudogap metal in both the nodal and antinodal regions of the Brillouin zone, as discussed in earlier work (24).
2. The parent pseudogap metal state already has a gap in the antinodal region of the electronic Brillouin zone. So, it is natural that this gap is preserved when the pseudogap metal undergoes a confinement transition to a charge-ordered state, potentially allowing us to understand the fermiology of the quantum oscillations.
3. The charge-ordered and d-wave superconducting confining states are not distinguished by the leading terms in the continuum static effective action for the chargons B. The degeneracy between these states is broken only by terms quartic in B, such as $v_{1,2,3}$ in Eq. **14**. This provides a rationale for the near-equality of the energy scales of charge-ordering and d-wave superconductivity (7).

Data, Materials, and Software Availability. There are no data underlying this work.

ACKNOWLEDGMENTS. We thank Darshan Joshi, Alexander Nikolaenko, and Jonas von Milczewski for useful discussions and earlier related collaborations. We also thank Shubhayu Chatterjee, Debanjan Chowdhury, Antoine Georges, Steven Kivelson, Patrick Lee, T. Senthil, and Shiwei Zhang for valuable discussions. S.S. thanks D.K. Sachdev for many discussions and dedicates this paper to his memory. This research was supported by the US NSF grant no. DMR-2002850 and by the Simons Collaboration on Ultra-Quantum Matter which is a grant from the Simons Foundation (651440, S.S.). The Flatiron Institute is a division of the Simons Foundation.

Author affiliations: [a]Department of Physics, Harvard University, Cambridge, MA 02138; [b]Center for Computational Quantum Physics, Flatiron Institute, New York, NY 10010; [c]Department of Physics and Astronomy, Johns Hopkins University, Baltimore, MD 21218; and [d]Institute for Theoretical Physics, University of Innsbruck, Innsbruck A-6020, Austria

1. B. Keimer, S. A. Kivelson, M. R. Norman, S. Uchida, J. Zaanen, From quantum matter to high-temperature superconductivity in copper oxides. *Nature* **518**, 179–186 (2015). 10.1038/nature14165.
2. M. Kyle *et al.*, Nodal quasiparticles and antinodal charge ordering in $Ca_{2-x}Na_xCuO_2Cl_2$. *Science*, **307**, 901–904 (2005).
3. H.-B. Yang *et al.*, Reconstructed fermi surface of underdoped $Bi_2Sr_2CaCu_2O_{8+\delta}$ cuprate superconductors. *Phys. Rev. Lett.* **107**, 047003 (2011). 10.1103/PhysRevLett.107.047003.
4. N. Doiron-Leyraud *et al.*, Quantum oscillations and the Fermi surface in an underdoped high-T_c superconductor. *Nature* **447**, 565–568 (2007).
5. N. Harrison, S. E. Sebastian, Protected nodal electron pocket from multiple-Q ordering in underdoped high temperature superconductors. *Phys. Rev. Lett.* **106**, 226402 (2011).
6. A. Allais, D. Chowdhury, S. Sachdev, Connecting high-field quantum oscillations to zero-field electron spectral functions in the underdoped cuprates. *Nat. Commun.* **5**, 5771 (2014).

7. F. Laliberté *et al.*, High field charge order across the phase diagram of $YBa_2Cu_3O_y$. *npj Quant. Mater.* **3**, 11 (2018). 10.1038/s41535-018-0084-5.
8. A. Nikolaenko, J. von Milczewski, D. G. Joshi, S. Sachdev, Spin density wave, Fermi liquid, and fractionalized phases in a theory of antiferromagnetic metals using paramagnons and bosonic spinons. arXiv [Preprint] (2022). http://arxiv.org/abs/2211.10452 (Accessed 2 May 2023).
9. Y.-H. Zhang, S. Sachdev, From the pseudogap metal to the Fermi liquid using ancilla qubits. *Phys. Rev. Res.* **2**, 023172 (2020).
10. Y.-H. Zhang, S. Sachdev, Deconfined criticality and ghost Fermi surfaces at the onset of antiferromagnetism in a metal. *Phys. Rev. B* **102**, 155124 (2020).
11. L. Zou, D. Chowdhury, Deconfined metallic quantum criticality: A $U(2)$ gauge-theoretic approach. *Phys. Rev. Res.* **2**, 023344 (2020).
12. S. Sachdev, Quantum phases of the Shraiman–Siggia model. *Phys. Rev. B* **49**, 6770–6778 (1994).
13. X.-G. Wen, P. A. Lee, Theory of underdoped cuprates. *Phys. Rev. Lett.* **76**, 503–506 (1996).
14. P. A. Lee, N. Nagaosa, T.-K. Ng, X.-G. Wen, SU(2) formulation of the t-J model: Application to underdoped cuprates. *Phys. Rev. B* **57**, 6003–6021 (1998).
15. P. A. Lee, N. Nagaosa, X.-G. Wen, Doping a Mott insulator: Physics of high-temperature superconductivity. *Rev. Mod. Phys.* **78**, 17 (2006). 10.1103/RevModPhys.78.17.
16. T. D. Stanescu, G. Kotliar, Fermi arcs and hidden zeros of the Green function in the pseudogap state. *Phys. Rev. B* **74**, 125110 (2006).
17. C. Berthod, T. Giamarchi, S. Biermann, A. Georges, Breakup of the Fermi surface near the Mott transition in low-dimensional systems. *Phys. Rev. Lett.* **97**, 136401 (2006).
18. K.-Y. Yang, T. M. Rice, F.-C. Zhang, Phenomenological theory of the pseudogap state. *Phys. Rev. B* **73**, 174501 (2006).
19. N. J. Robinson, P. D. Johnson, T. Maurice Rice, A. M. Tsvelik, Anomalies in the pseudogap phase of the cuprates: Competing ground states and the role of umklapp scattering. *Rep. Progr. Phys.* **82**, 126501 (2019).
20. R. K. Kaul, Y. B. Kim, S. Sachdev, T. Senthil, Algebraic charge liquids. *Nat. Phys.* **4**, 28–31 (2008).
21. S. Sakai, Y. Motome, M. Imada, Evolution of electronic structure of doped Mott insulators: Reconstruction of poles and zeros of Green's function. *Phys. Rev. Lett.* **102**, 056404 (2009).
22. Y. Qi, S. Sachdev, Effective theory of Fermi pockets in fluctuating antiferromagnets. *Phys. Rev. B* **81**, 115129 (2010).
23. J.-W. Mei, S. Kawasaki, G.-Q. Zheng, Z.-Y. Weng, X.-G. Wen, Luttinger-volume violating Fermi liquid in the pseudogap phase of the cuprate superconductors. *Phys. Rev. B* **85**, 134519 (2012).
24. E. Mascot *et al.*, Electronic spectra with paramagnon fractionalization in the single-band Hubbard model. *Phys. Rev. B* **105**, 075146 (2022).
25. J. Skolimowski, M. Fabrizio, Luttinger's theorem in the presence of Luttinger surfaces. *Phys. Rev. B* **106**, 045109 (2022).
26. T. Senthil, S. Sachdev, M. Vojta, Fractionalized Fermi liquids. *Phys. Rev. Lett.* **90**, 216403 (2003).
27. T. Senthil, M. Vojta, S. Sachdev, Weak magnetism and non-Fermi liquids near heavy-fermion critical points. *Phys. Rev. B* **69**, 035111 (2004).
28. I. Affleck, J. Brad Marston, Large-*n* limit of the Heisenberg–Hubbard model: Implications for high-T_c superconductors. *Phys. Rev. B* **37**, 3774–3777 (1988). 10.1103/PhysRevB.37.3774.
29. C. Wang, A. Nahum, M. A. Metlitski, C. Xu, T. Senthil, Deconfined quantum critical points: Symmetries and dualities. *Phys. Rev. X* **7**, 031051 (2017).
30. N. Read, S. Sachdev, Valence-bond and spin-Peierls ground states of low-dimensional quantum antiferromagnets. *Phys. Rev. Lett.* **62**, 1694–1697 (1989). 10.1103/PhysRevLett.62.1694.
31. I. Affleck, Z. Zou, T. Hsu, P. W. Anderson, SU(2) gauge symmetry of the large-*U* limit of the Hubbard model. *Phys. Rev. B* **38**, 745–747 (1988). 10.1103/PhysRevB.38.745.
32. E. Dagotto, E. Fradkin, A. Moreo, SU(2) gauge invariance and order parameters in strongly coupled electronic systems. *Phys. Rev. B* **38**, 2926–2929 (1988). 10.1103/PhysRevB.38.2926.
33. A. Tanaka, X. Hu, Many-body spin berry phases emerging from the π-flux state: Competition between antiferromagnetism and the valence-bond-solid state. *Phys. Rev. Lett.* **95**, 036402 (2005).
34. M. Hermele, T. Senthil, M. P. A. Fisher, Algebraic spin liquid as the mother of many competing orders. *Phys. Rev. B* **72**, 104404 (2005).
35. T. Senthil, M. P. A. Fisher, Competing orders, nonlinear sigma models, and topological terms in quantum magnets. *Phys. Rev. B* **74**, 064405 (2006).
36. Y. Ran, X.-G. Wen, Continuous quantum phase transitions beyond Landau's paradigm in a large-*N* spin model. arXiv [Preprint] (2006). https://doi.org/10.48550/arXiv.cond-mat/0609620 (Accessed 2 May 2023).
37. Y. Ran, "Spin liquids, exotic phases and phase transitions," PhD thesis, MIT, Cambridge, MA (2007).
38. P. W. Anderson, The resonating valence bond state in La_2CuO_4 and superconductivity. *Science* **235**, 1196–1198 (1987). 10.1126/science.235.4793.1196.
39. G. Baskaran, Z. Zou, P. W. Anderson, The resonating valence bond state and high-T_c superconductivity–A mean field theory. *Solid State Commun.* **63**, 973–976 (1987). https://www.sciencedirect.com/science/article/pii/0038109887906429.
40. A. E. Ruckenstein, P. J. Hirschfeld, J. Appel, Mean-field theory of high-T_c superconductivity: The superexchange mechanism. *Phys. Rev. B* **36**, 857–860 (1987). 10.1103/PhysRevB.36.857.
41. F. C. Zhang, C. Gros, T. M. Rice, H. Shiba, A renormalised Hamiltonian approach for a resonant valence bond wavefunction. *Supercond. Sci. Technol.* **1**, 36 (1988).
42. G. Kotliar, J. Liu, Superexchange mechanism and *d*-wave superconductivity. *Phys. Rev. B* **38**, 5142–5145 (1988). 10.1103/PhysRevB.38.5142.
43. D. A. Ivanov, T. Senthil, Projected wave functions for fractionalized phases of quantum spin systems. *Phys. Rev. B* **66**, 115111 (2002).
44. A. Nikolaenko, M. Tikhanovskaya, S. Sachdev, Y.-H. Zhang, Small to large Fermi surface transition in a single band model, using randomly coupled ancillas. *Phys. Rev. B* **103**, 235138 (2021).
45. S. Florens, A. Georges, Slave-rotor mean-field theories of strongly correlated systems and the Mott transition in finite dimensions. *Phys. Rev. B* **70**, 035114 (2004).
46. L. Balents, L. Bartosch, A. Burkov, S. Sachdev, K. Sengupta, Putting competing orders in their place near the Mott transition. *Phys. Rev. B* **71**, 144508 (2005).
47. X.-Y. Song , Y.-H. Zhang , Deconfined criticalities and dualities between chiral spin liquid, topological superconductor and charge density wave Chern insulator. arXiv [Preprint] (2022). http://arxiv.org/abs/2206.08939 (Accessed 2 May 2023).
48. S. Chakravarty, R. B. Laughlin, D. K. Morr, C. Nayak, Hidden order in the cuprates. *Phys. Rev. B* **63**, 094503 (2001).
49. R. Ma, C. Wang, Theory of deconfined pseudocriticality. *Phys. Rev. B* **102**, 020407 (2020).
50. A. Nahum, Note on Wess–Zumino–Witten models and quasiuniversality in 2+1 dimensions *Phys. Rev. B* **102**, 201116 (2020).
51. Z. Wang, M. P. Zaletel, R. S. K. Mong, F. F. Assaad, Phases of the $(2+1)$ dimensional SO(5) nonlinear sigma model with topological term *Phys. Rev. Lett.* **126**, 045701 (2021).
52. Y.-C. He, J. Rong, S. Ning, Non-Wilson–Fisher kinks of O(*N*) numerical bootstrap: From the deconfined phase transition to a putative new family of CFTs. *Sci. Post. Phys.* **10**, 115 (2021).
53. Z. Li, Bootstrapping conformal QED3 and deconfined quantum critical point. *J. High Energy Phys.* **2022**, 5 (2022). 10.1007/JHEP11(2022)005.
54. T. Senthil, A. Vishwanath, L. Balents, S. Sachdev, M. P. A. Fisher, Deconfined quantum critical points. *Science* **303**, 1490–1494 (2004).
55. F. F. Assaad, M. Imada, D. J. Scalapino, Quantum transition between an antiferromagnetic Mott insulator and $d_{x^2-y^2}$ superconductor in two dimensions. *Phys. Rev. Lett.* **77**, 4592–4595 (1996).
56. M. Imada, Charge order and superconductivity as competing brothers in cuprate high-T_c superconductors. *J. Phys. Soc. Japan* **90**, 111009 (2021).
57. S.-C. Zhang, A unified theory based on SO(5) symmetry of superconductivity and antiferromagnetism. *Science* **275**, 1089 (1997).
58. L. Balents, L. Bartosch, A. Burkov, S. Sachdev, K. Sengupta, Putting competing orders in their place near the Mott transition. II. The doped quantum dimer model. *Phys. Rev. B* **71**, 144509 (2005).
59. L. Balents, S. Sachdev, Dual vortex theory of doped Mott insulators. *Ann. Phys.* **322**, 2635–2664 (2007).
60. Y. Ran, A. Vishwanath, D.-H. Lee, A direct transition between a Neel ordered Mott insulator and a $d_{x^2-y^2}$ superconductor on the square lattice. arXiv [Preprint] (2008). http://arxiv.org/abs/0806.2321 (Accessed 2 May 2023).
61. S. Raghu, S. A. Kivelson, D. J. Scalapino, Superconductivity in the repulsive Hubbard model: An asymptotically exact weak-coupling solution. *Phys. Rev. B* **81**, 224505 (2010).
62. M. A. Metlitski, S. Sachdev, Quantum phase transitions of metals in two spatial dimensions: II. Spin density wave order. *Phys. Rev. B* **82**, 075128 (2010).
63. M. A. Metlitski, S. Sachdev, Instabilities near the onset of spin density wave order in metals. *New J. Phys.* **12**, 105007 (2010). 10.1088/1367-2630/12/10/105007.
64. A. Jaefari, S. Lal, E. Fradkin, Charge-density wave and superconductor competition in stripe phases of high-temperature superconductors. *Phys. Rev. B* **82**, 144531 (2010).
65. E. Fradkin, S. A. Kivelson, J. M. Tranquada, Colloquium: Theory of intertwined orders in high temperature superconductors. *Rev. Mod. Phys.* **87**, 457–482 (2015).
66. K. B. Efetov, H. Meier, C. Pépin, Pseudogap state near a quantum critical point. *Nat. Phys.* **9**, 442–446 (2013). 10.1038/nphys2641 (Accessed 2 May 2023).
67. C. Pépin , H. Freire , Charge order and emergent symmetries in cuprate superconductors. arXiv [Preprint] (2022). http://arxiv.org/abs/2210.04046 (Accessed 2 May 2023).
68. L. E. Hayward, D. G. Hawthorn, R. G. Melko, S. Sachdev, Angular fluctuations of a multi-component order describe the pseudogap regime of the cuprate superconductors. *Science* **343**, 1336 (2014).
69. L. Nie, L. E. Hayward Sierens, R. G. Melko, S. Sachdev, S. A. Kivelson, Fluctuating orders and quenched randomness in the cuprates. *Phys. Rev. B* **92**, 174505 (2015).
70. S. Chatterjee, Y. Qi, S. Sachdev, J. Steinberg, Superconductivity from a confinement transition out of a fractionalized Fermi liquid with Z_2 topological and Ising-nematic orders. *Phys. Rev. B* **94**, 024502 (2016).
71. S. Chatterjee, S. Sachdev, Fractionalized Fermi liquid with bosonic chargons as a candidate for the pseudogap metal. *Phys. Rev. B* **94**, 205117 (2016).
72. S. Sachdev, H. D. Scammell, M. S. Scheurer, G. Tarnopolsky, Gauge theory for the cuprates near optimal doping. *Phys. Rev. B* **99**, 054516 (2019).
73. P. M. Bonetti, W. Metzner, SU(2) gauge theory of the pseudogap phase in the two-dimensional Hubbard model. *Phys. Rev. B* **106**, 205152 (2022).
74. B. Dalla Piazza *et al.*, Fractional excitations in the square-lattice quantum antiferromagnet. *Nat. Phys.* **11**, 62–68 (2015).
75. N. S. Headings, S. M. Hayden, R. Coldea, T. G. Perring, Anomalous High-Energy Spin Excitations in the High-T_c Superconductor-Parent Antiferromagnet $La_2\ CuO_4$. *Phys. Rev. Lett.* **105**, 247001 (2010).
76. M. Hering, J. Sonnenschein, Y. Iqbal, J. Reuther, Characterization of quantum spin liquids and their spinon band structures via functional renormalization. *Phys. Rev. B* **99**, 100405 (2019).
77. X.-Y. Song, Y.-C. He, A. Vishwanath, C. Wang, From spinon band topology to the symmetry quantum numbers of monopoles in Dirac spin liquids. *Phys. Rev. X* **10**, 011033 (2020).
78. A. A. Patel, D. Chowdhury, A. Allais, S. Sachdev, Confinement transition to density wave order in metallic doped spin liquids. *Phys. Rev. B* **93**, 165139 (2016).
79. J. M. Tranquada, B. J. Sternlieb, J. D. Axe, Y. Nakamura, S. Uchida, Evidence for stripe correlations of spins and holes in copper oxide superconductors. *Nature* **375**, 561–563 (1995). 10.1038/375561a0.
80. S. Weinberg, A model of leptons. *Phys. Rev. Lett.* **19**, 1264–1266 (1967). 10.1103/PhysRevLett.19.1264.
81. S. Gazit, M. Randeria, A. Vishwanath, Emergent Dirac fermions and broken symmetries in confined and deconfined phases of Z2 gauge theories. *Nat. Phys.* **13**, 484–490 (2017). 10.1038/nphys4028.
82. S. Gazit, F. F. Assaad, S. Sachdev, A. Vishwanath, C. Wang, Confinement transition of $\mathbb{Z}_2$ gauge theories coupled to massless fermions: Emergent quantum chromodynamics and SO(5) symmetry. *Proc. Natl. Acad. Sci. U.S.A.* **115**, E6987–E6995 (2018).
83. S. Gazit, F. F. Assaad, S. Sachdev, Fermi surface reconstruction without symmetry breaking. *Phys. Rev. X* **10**, 041057 (2020).
84. H.-C. Jiang, S. A. Kivelson, High temperature superconductivity in a lightly doped quantum spin liquid. *Phys. Rev. Lett.* **129**, 097002 (2021).
85. H.-C. Jiang , S. A. Kivelson , D.-H. Lee , Superconducting valence bond fluid in lightly doped 8-leg *t-J* cylinders. arXiv [Preprint] (2023). https://arxiv.org/abs/2302.11633 (Accessed 1 May 2023).
86. E. Fradkin, S. H. Shenker, Phase diagrams of lattice gauge theories with Higgs fields. *Phys. Rev. D* **19**, 3682–3697 (1979). 10.1103/PhysRevD.19.3682.